High-conductivity Hydrophobic Fumed-SiO$_2$ Composite Gel Electrolyte for High Performance Electrochromic Devices

ZHAO Qi[1], QIAO Ke[1], YAO Yongji[1], CHEN Zhang[1], CHEN Dongchu[2], GAO Yanfeng[1]

(1. School of Materials Science and Engineering, Shanghai University, Shanghai 200444, China; 2. School of Materials Science and Energy Engineering, Foshan University, Foshan 528000, China)

Abstract: Gel electrolytes are chemically stable, nonflammable and easy to encapsulate, however, their moderate ionic conductivity (10^{-4}–10^{-5} S·cm^{-1}) hinders their further development for the usage in electrochromic devices (ECDs). Here, we developed a highly conductive hydrophobic SiO$_2$/PMMA/PC/LiClO$_4$ gel polymer electrolyte (H-SiO$_2$ GPE). Electrochemical behaviors of ECDs were characterized by electrochemical impedance spectroscope (EIS), cyclic voltammetry (CV) and chronoamperometry (CA). Systematic analyses show that the ionic conductivity of the H-SiO$_2$ GPE can reach 5.14 mS·cm^{-1} (at 25 ℃) by introducing only 0.5wt% hydrophobic fumed SiO$_2$. This increase is due to the good compatibility and hydrophobic-hydrophobic attractions between SiO$_2$ additive and organic electrolyte, which promotes the dissociation of lithium perchlorate. Additionally, the viscosity as a function of shear rate for GPE with various fumed silica contents shows the behavior of shear thinning, which indicates the formation of a three-dimensional network structure. This structure provides ion transport channels, leading to a clearly improved switching speed for ECDs assembled with hydrophobic SiO$_2$ GPEs ($t_{bleaching}$=4 *vs* 8 s and $t_{coloring}$=14 *vs* 16 s). Similarly, the investigation of hydrophobic fumed SiO$_2$ in liquid electrolyte is demonstrated that the ionic conductivity of LiClO$_4$/PC liquid electrolyte without and with hydrophobic fumed SiO$_2$ increases from 6.94 to 7.58 mS·cm^{-1}, respectively. Therefore, hydrophobic fumed SiO$_2$ as a filler has a positive effect on electrolytes, and the proposal of the H-SiO$_2$ GPE provides a new idea for offsetting the trade-off between a high ionic conductivity and easy leakage when applied in ECDs.

Key words: gel electrolyte; electrochromic; hydrophobic; SiO$_2$

Electrochromic devices (ECDs) can reversibly change their light transmittance *via* external voltage-induced redox reactions, and show potential applications in smart windows, electrochromic displays, switching mirrors, sensors, supercapacitors and so on[1]. To stabilize ECDs, the internal resistance of ECDs must be remarkably reduced, which requires anionic conductivity higher than 1 mS·cm^{-1}[2]. Liquid electrolytes usually deliver high conductivity and high switching speed[3], but ECDs using liquid electrolytes suffer from persistent problems, such as electrolyte leakage, flammability and chemical stability issues.

To overcome the above mentioned problems, gel polymer electrolytes (GPEs) have been developed; these GPEs generally show a much higher conductivity than solid polymer electrolytes (> 10^{-4} *vs* 10^{-8} S·cm^{-1})[4]. GPEs refer to a family of polymer-based electrolytes that are prepared by dissolving polymer matrices into liquid electrolytes or trapping liquid electrolytes into the network of polymer matrices[5]. The most commonly used matrices in GPEs are poly(ethylene oxide) (PEO)[6], poly(acrylonitrile) (PAN)[7], poly(vinylidene fluoride) (PVDF)[8], poly (vinylidene fluoride-hexafluoropropylene) (PVDF-HFP)[9] and polymethyl methacrylate (PMMA)[2,8], additionally,

the common plasticizers are propylene carbonate (PC), ethylene carbonate (EC), ethyl methyl carbonate (EMC) or their mixtures. The crystalline structure of the matrices provides the backbone of the gel, and the amorphous phase of the matrices forms the continuous phase to transport ions in the GPEs.

It is well accepted that fillers play an important role in Li^+ transport, but the apparent discrepancy in electro-chemical performances can partially be ascribed to the difference in electrolyte materials (polymers, salt, filler type), along with their concentration and preparation conditions. The addition of nanoparticles (such as TiO_2[10], CeO_2[11], Al_2O_3[12], and palygorskite[13]) can not only improve the mechanical strength of GPEs, but also increase their conductivity by increasing the volume fraction of the amorphous phase. However, the ionic conductivity of these composite electrolytes ranges from 10^{-4} to 10^{-5} S·cm^{-1} at ambient temperature, which is still too low for commercial applications[14].

Fumed SiO_2 has been widely adopted as a filler to improve the conductivity and mechanical stability of GPEs, because of its branched three-dimensional structure and the flexibly-tunable surface functionalities[10]. Currently, most studies are conducted on the development of hydro-philic fumed SiO_2 as GPEs additive (with a large amount of silanol groups on the surface), because of its ionizing lithium salt and ability to increase the amorphous phase content of the polymer matrix. However, hydrophilic SiO_2 with polar silanol groups tends to aggregate[15].Moreover, hydrophilic SiO_2 presents a low compatibility with organic GPEs. Therefore, employing hydrophobic SiO_2 may be a better choice for their application in GPEs due to its high dispersibility in organic matrices.

In this study, we investigate the effect of a hydrophobic fumed SiO_2/PMMA/PC/LiClO$_4$ GPE (H-SiO$_2$ GPE) and their applications in ECDs. It is demonstrated that hydro-phobic fumed SiO_2 is more efficient in increasing the ionic conductivity of electrolytes, because of the hydrophobic-hydrophobic attractions between the hydrophobic groups on the SiO_2 surfaces and solvents in the GPE.The ECD assembled with H-SiO$_2$ GPE exhibits a fast switching speed ($t_{bleaching}$=4 vs 8 s and $t_{coloring}$=14 vs 16 s). To compare, the effect of a hydrophobic fumed SiO_2/LiClO$_4$/ PC/liquid electrolyte is explored. This work demonstrates that the addition of hydrophobic fumed SiO_2 in elec-trolytes provides great potential for the application in ECDs and other energy devices.

1 Experimental

1.1 Chemicals

Propylene carbonate (PC, 99%), lithium perchlorate (LiClO$_4$, 99.9%), hydrophobic fumed SiO_2 (Aladdin, 7-40 nm, pH=4.5), polymethyl methacrylate (PMMA, Aldrich, Mw≈1000, 000) were obtained and used.

1.2 Preparation of the liquid electrolytes and GPEs

The liquid electrolyte was prepared by dissolving 0.1 mol·L^{-1} LiClO$_4$ in 7.41 mL propylene carbonate under stirring. Afterward, 0, 20, 50, 80 and 100 mg of hydro-phobic fumed SiO_2 was dispersed into 10 g of liquid electrolyte with ultrasonication. This process provided hydrophobic fumed SiO_2/LiClO$_4$/PC liquid electrolyte with 0, 0.2wt%, 0.5wt%, 0.8wt% and 1.0wt% fumed SiO_2. Hydrophobic fumed SiO_2/polymethyl methacrylate (PMMA)/PC/LiClO$_4$ GPEs (H-SiO$_2$ GPEs) were prepared by dissolving 1 g of PMMA (vacuum dried at 90 ℃ for 24 h) into 9 g of liquid electrolyte under stirring at 90 ℃.

1.3 Preparation of the WO$_3$ nanopowder

WO$_3$ nanoparticles were synthesized using the reported hydrothermal process[16]. In a typical experiment, 0.815 g of Na$_2$WO$_4$·2H$_2$O was dissolved in 10 mL of deionized water. Then the Na$_2$WO$_4$ solution was acidified to pH 2.0 using HCl solution at room temperature. Afterward, the solution was transferred into a Teflon-lined autoclave and heat-treated at 180 ℃ for 24 h. Finally, the final products were sequentially washed with deionized water and ethanol to remove the sulfate ions and other remnants by centrifugation.

1.4 Assembly of ECDs based on different electrolytes

WO$_3$ electrochromic films were deposited on clean ITO glasses by a wire-bar coating method, as reported in our previous work[17]. When using the liquid electrolytes, the ECDs were sealed with 3M tape while leaving one small gap in which the LiClO$_4$/PC liquid electrolytes (with/without hydrophobic fumed SiO_2) were injected into the device by a syringe. Finally, the injection ports were sealed with UV curing glue. In regard to the GPEs, GPEs with/without hydrophobic fumed SiO_2 were cast into WO$_3$ electrochromic layers, and finally, these ECDs were also sealed with 3M tape.

1.5 Characterization

Viscosity measurements were determined by rotary rheometer (HAAKE MARS60) under shear rate of 0.1– 100 s^{-1} at room temperature. The morphology of WO$_3$ films was characterized by scanning electron microscope (SEM, S-4800, Hitachi, Tokyo, Japan) and transmission electron microscope (TEM, JEOL, JEM-2100, 200 kV). The morphologies of the gel electrolyte were characterized by FE-SEM (JEOL, JSM6700F, Tokyo). The crystal structure of the electrochromic film was required by X-ray diffraction (XRD; 3kW Bruker D8 Advance X-ray

diffractometer with Cu Kα irradiation, $\lambda=0.154$ nm). The optical transmittance of the electrochromic devices was characterized by UV spectrophotometer (UH4150; Hitachi, Japan) at 633 nm. The ionic conductivity was measured by Mettler Seven compact conductivity meter. Electrochemical measurements were performed on electrochemical workstation (CHI760E, CHI Instruments, China). Electrochemical impedance spectroscopy (EIS) of the electrochromic film was recorded from 10^{-1} to 10^{6} Hz at an amplitude of 5 mV.

2   Results and discussion

2.1   Phase characterization

The hydrophobicity of SiO_2 is investigated by the contact angle test, as presented in Fig. S1. Regardless of how the needle moves, water droplets cannot adhere to the surface of hydrophobic fumed SiO_2. Fig. 1 shows the FT-IR spectrum of the hydrophobic fumed SiO_2. The broad peaks at 3446 and 1631 cm^{-1} are the –OH stretching and bending vibration peaks of adsorbed water, respectively. The peaks at 808 and 478 cm^{-1} are the symmetric stretching vibrations and bending vibrations of Si–O bonds. The strong and wide absorption band at 1110 cm^{-1} is the anti-symmetric stretching vibration peak of Si–O–Si. The peak at 979 cm^{-1} is the stretching vibration of Si–OH, indicating the possibility for further reaction as a proton donor[18]. Peaks at 2976, 2927, and 2856 cm^{-1} are the stretching vibration peaks of the –CH₃, and –CH₂– groups. Due to the existence of –CH₃, –CH₂– terminals, this fumed SiO_2 shows hydrophobic properties and good dispersibility in organic matrices, as revealed in Fig. S2. The particle size distribution of hydrophilic fumed SiO_2 shows two peaks in PC, and a strong peak in the range of 1000–10000 nm. These results indicate that hydrophilic fumed –SiO_2 can agglomerate in PC. In contrast, hydrophobic fumed-SiO_2 is mainly distributed between 100 and 1000 nm. It can be concluded that the hydrophobic fumed SiO_2 has better uniformity in PC. The scanning electron micr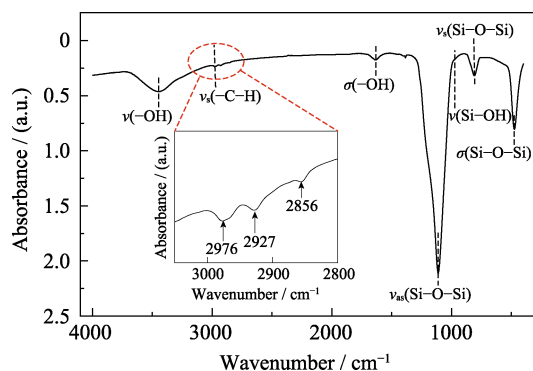ographs of the prepared pure GPEs and H-SiO_2 GPEs are shown in Fig. S3. H–SiO_2 evenly distributes in the main body of the GPEs.

2.2   Effect of fumed SiO₂ on the Gel electrolyte and electrochromic devices

2.2.1   Measurements of the ionic conductivities of H-SiO₂ GPEs

A high ionic conductivity facilitates the transportation of ions into and out of an EC film to initiate a color change, which is the key indicator of an electrolyte. The ionic conductivities of these GPEs are calculated by the formula $\sigma = L/R_bA$, where L is the thickness of the GPE electrolyte, A is the contact area between the electrolyte and the electrode, and the bulk resistance (R_b) is the intercept of the curve and the Z' axis in the AC impedances (Fig. 2(a))[19]. The measurement was conducted at 25 ℃ and 40% humidity. The experiments were repeated three times to reduce the measuring and experimental error, and an average value was obtained for the final results. The conductivity of the H-SiO_2 GPE first increases and then decreases with an increasing concentration of fumed SiO_2. The GPE shows a maximum conductivity of 5.14 mS·cm^{-1} at 0.5wt% concentration of fumed SiO_2 (Fig. 2(b)), which is clearly higher than the previously reported values in the literature (Table S1). The conductivity evolution of the GPEs with different SiO_2 concentrations can be explained by the trade-off between the improved dissociation of lithium perchlorate and the increase in viscosity (Fig. 2(c)). Specifically, there are a large number of methyl groups on the surface of hydrophobic SiO_2, which is the main reason for its hydrophobicity. These methyl groups can form mutual hydrophobic-hydrophobic attractions with the organic groups in organic solvents to promote the dispersion of SiO_2, thus improving the dissociation of lithium perchlorate and providing the GPE a high transparency. Moreover, it is noted that the polarity difference between SiO_2 with a large number of hydroxyl groups and an organic electrolyte can affect the dispersion of SiO_2 in PMMA matrices[15], further decreasing the ionic conductivity (Table 1). Additionally, as the viscosity continues to increase, the polar end of the molecule is gradually adsorbed on the silica surface, which halts further network formation at this site and hinders the motion of Li⁺.

2.2.2   Electrochromic performances of ECDs based on H-SiO₂ GPEs

To explore the effect of H-SiO_2 GPEs on electrochromism, the ECDs were assembled by WO_3 coated on ITO glass[17] and using GPEs with/without hydrophobic fumed SiO_2. The specific details of WO_3 are shown in Fig. S4. The electrochemical behaviors of the ECDs were characterized by electrochemical impedance spectroscopy in the colored state (EIS, Fig. 2(d)). Each of the EIS
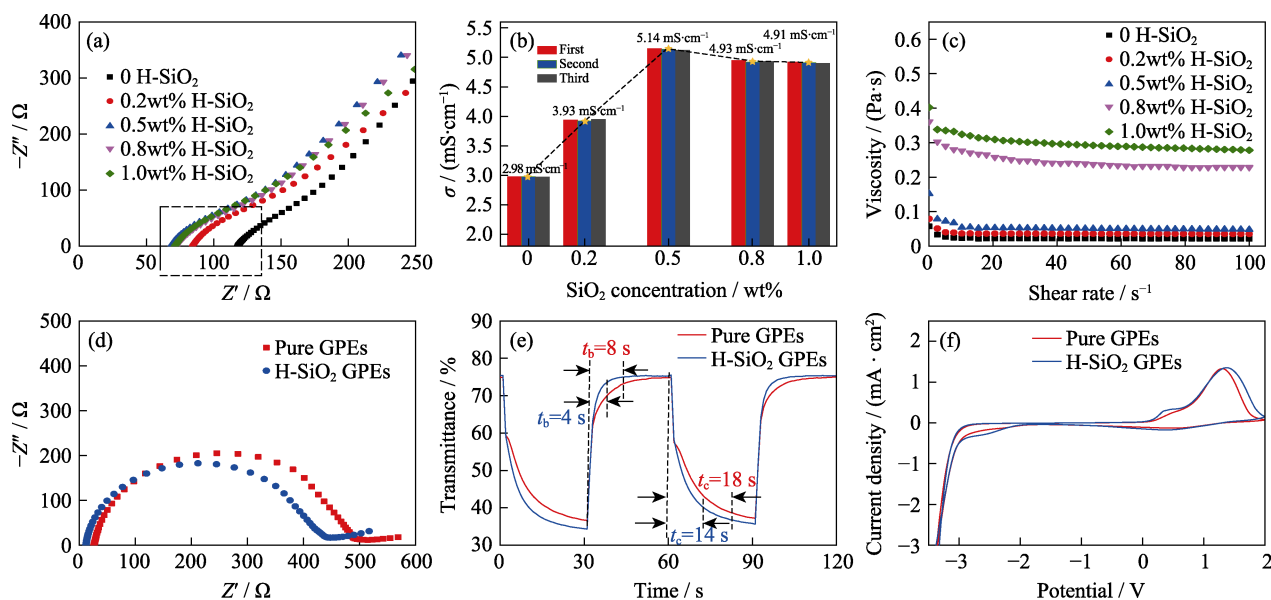

Fig. 1   FT-IR spectrum of hydrophobic fumed SiO₂

Fig. 2 Nyquist plots (a), ionic conductivity (b) and viscosity (c) of PMMA-based GPEs with 0, 0.2wt%, 0.5wt%, 0.8wt% and 1.0wt% fumed SiO₂. Electrochromic switching behaviors at 633 nm (e), colored state EIS (d) and CV curves (f) of ECDs contained PMMA-based GPEs with 0, 0.5wt% fumed SiO₂. Scan rate: 100 mV/s

spectra is composed of a semicircle part at high frequencies and a diagonal part at low frequencies. The semicircle part reflects the charge transfer resistance between the electrochromic film and electrolyte. The diagonal part represents the Warburg impedance that is associated with the ion diffusion process. In other words, the larger the slope of the line is, the faster the ion transfer process. Therefore, it is obvious that the resistance is low and the ion diffusion is good with H-SiO₂ GPEs.

To further investigate the electrochromic performances of ECDs, as shown in Fig. 2(e). An ECD with H-SiO₂ GPEs switches faster than that without SiO₂. More precisely, the switching time sare 16/14 s (coloring) and 8/4s (bleaching) for ECDs with pure GPEs and H-SiO₂ GPEs, respectively. Compared with other similar constructions of ECDs (using WO₃, ITO glass and a gel electrolyte as electrochromic layers, substrates and ion transport layers, respectively), H-SiO₂ GPEs exhibit faster speeds than previously reported results for PVdF-HFP-based ($t_{coloring}=17$ s/$t_{bleaching}=28$ s)[20], PMMA-based ($t_{coloring}=62.6$ s/$t_{bleaching}=41.2$ s)[21], ionic-liquid-based ($t_{coloring}=15$ s/$t_{bleaching}=15$ s)[22] and PVB-based ($t_{coloring}=16.5$ s/$t_{bleaching}=9.5$ s)[23] gel electrolytes. In addition, the transmittance modulation of ECDs increases from 38.3% to 41.2%, which is higher than that reported above (41.2% vs 35%[20] vs 24%[22] vs 18%[19]). The enhanced electrochromic performance can be attributed to the above mentioned high ionic conductivity and shear thinning behavior. The viscosity follows a linear correlation with respect to the shear rate. The viscosity as a function of shear rate for the GPE with various fumed silica contents is shown in

Fig. 2(c). At a low shear rate, it exhibits a solid-like behavior with a high viscosity value due to the formation of a network structure by the induction of a siloxane linkage in the polymer matrix. At a high shear rate, because the orientation of the siloxane linkage is preferential parallel to the flow direction, the viscosity decreases. Shear thinning occurs because the bonds composing the network structure are physically weak, which can be disturbed by shear[24]. Thus, the H-SiO₂ GPEs are proven to be physical gels with a three-dimensional network[14]. As presented in Fig. 3, hydrophobic fumed SiO₂ can be attracted to the PMMA chains, forming a three-dimensional network structure, while providing ion transport channels so that ions can transport more quickly and easily to the interface of the WO₃ films and electrolyte.
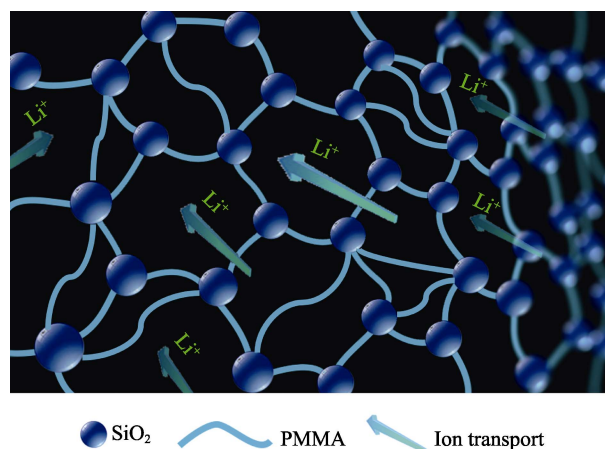

Fig. 3 Schematic diagram of the transportation of Li⁺ ion through H-SiO₂GPEs with three-dimensional structure

In addition, the CV curves of the ECDs with different GPEs are shown in Fig. 2(f). The CV curve of the SiO$_2$-free ECD has a cathode current peak at -3.3 V and an anodic current peak at 1.3 V. In contrast, the CV curves of the SiO$_2$ containing ECDs show cathode current peaks at $+0.37$ V, and anodic current peaks at -2.6 V. These new peaks may be attributed to different binding sites on the WO$_3$ film[25], indicating a better reactivity of the electrochromic WO$_3$ films at a low bias voltage. According to a previous report[26], the introduction of cations can decrease the reaction voltage of WO$_3$. The addition of fumed SiO$_2$ enhances the concentration of Li$^+$ near the WO$_3$ film, thus leading to better electrochromic performance.

2.3 Effect of fumed SiO₂ on the liquid electrolyte and electrochromic devices

For a LiClO$_4$/PC liquid electrolyte, the PC solvent has a strong solvation effect on Li$^+$ cations, but the perchlorate anions are difficult to coordinate or solvate, limiting the achievement of high conductivity in this system. The conductivity of liquid electrolytes was measured by a conductivity meter, and the results show a similar trend to that of gel electrolytes. To increase the accuracy of data, the experiment was repeated three times (Fig. 4(a)). With SiO$_2$ additives from 0 to 0.5wt%, the ionic conductivity of the liquid electrolyte increases up to a maximum of 7.58 mS·cm^{-1}, which is higher than hydrophilic fumed SiO$_2$ or other additives as fillers (no more than 7.0 mS·cm^{-1})[10,14]. The increase of conductivity can be attributed to the reasons discussed in the section on GPEs. The good dispersion of hydrophobic fumed SiO$_2$ homogenizes the electrical field[27]. However, further increasing the SiO$_2$ concentration leads to a decrease in conductivity, possibly due to the increase in electrolyte viscosity and the aggregation of fumed SiO$_2$.

The effects of the hydrophobic fumed SiO$_2$ composite electrolyte on the electrochemical behaviors of WO$_3$ films were characterized by electrochemical impedance spectroscopy in the colored state (EIS, Fig. 4(b)). As shown in Fig. 4(b), both the charge transfer resistance and ion diffusion resistance reach a minimum at a SiO$_2$ concentration of 0.5wt%, which is consistent with the conductivity variation. Fig. 4(c) further presents the CV curves of the WO$_3$ films in SiO$_2$ electrolytes at different concentrations. In all of CV curves, clear cathodic current peaks appear with potential sweeping from $+1$ V to -1 V. Moreover, the colorless WO$_3$ film appears blue, due to the reduction of W$^{6+}\rightarrow$W^{5+} after Li$^+$ insertion. The film returns to be colorless after reverse sweeping the potential back to $+1$ V, suggesting the occurrence of the W$^{5+}\rightarrow$W^{6+} oxidation reaction accompanied by Li$^+$ extraction. Therefore, the WO$_3$ film demonstrates the largest CV curve in the highly conductive electrolyte containing the addition of 0.5wt% fumed SiO$_2$, confirming the beneficial influence of the fumed SiO$_2$ additive on the electrochemical reactions of the WO$_3$ film.

3 Conclusion

In conclusion, the introduction of hydrophobic fumed SiO$_2$ into GPEs can effectively increase the conductivity from 3.99 to 5.14 mS·cm^{-1}, because of the attractive force of hydrophobic groups. These interactions are beneficial for increasing the compatibility between SiO$_2$ and GPEs, thereby promoting the dissociation of lithium perchlorate, and improving the ionic conductivity. The assembled ECDs using H-SiO$_2$ GPEs exhibit lower cathode interface impedances, better electrochemical behaviors, and faster switching times, as compared with those of the unmodified GPEs ($t_{\text{bleaching}}=4$ *vs* 8 s and $t_{\text{coloring}}=14$ *vs* 16 s). These observations are owing to that H-SiO$_2$ GPEs form a three-dimensional network structure, thereby providing an ion transport channel. Similarly, the ionic conductivity of the LiClO$_4$/PC/liquid electrolyte without/with hydrophobic fumed SiO$_2$ increases from 6.94 mS·cm^{-1} (without hydrophobic fumed SiO$_2$) to 7.58 mS·cm^{-1}. This work demonstrates that the introduction of hydrophobic SiO$_2$ has a positive effect on electrolytes, which is an important step for their application in ECDs.
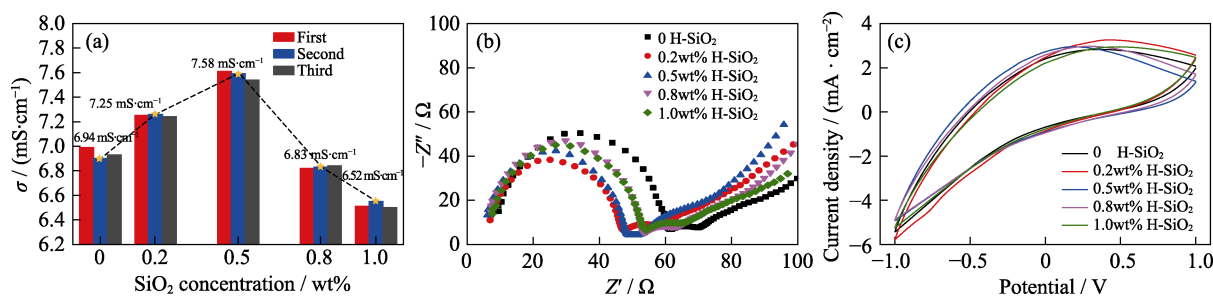

Fig. 4   Ionic conductivity of liquid electrolyte with 0, 0.2wt%, 0.5wt%, 0.8wt%, and 1.0wt% fumed SiO$_2$ (a), and colored state Nyquist plots (b) and CV curves (c) of WO$_3$ films in liquid electrolyte with 0, 0.2wt%, 0.5wt%, 0.8wt% and 1.0wt% fumed SiO$_2$. Scan rate: 100 mV/s

Supporting materials:

Supporting materials related to the article can be found at https://doi.org/10.15541/jim20200376.

References:

[1] PATEL K J, BHATT G G, RAY J R, et al. All-inorganic solid-state electrochromic devices: a review. *Journal of Solid State Electro-chemistry*, 2016, **21(2):** 1–11.

[2] AGNIHOTRYA SA, SEKHON P SS. PMMA based gel electrolyte for EC smart windows. *Electrochimica Acta*, 1998, **44:** 3121–3126.

[3] LI H, WANG J, SHI Q, et al. Constructing three-dimensional quasi-vertical nanosheet architectures from self-assemble two-dimensional $WO_3 \cdot 2H_2O$ for efficient electrochromic devices. *Applied Surface Science*, 2016, **380:** 281–287.

[4] GROCE F, APPETECCHI G B, PERSI L, et al. Nanocomposite polymer electrolytes for lithium batteries. *Nature*, 1998, **394:** 456.

[5] AZIZ S B, WOO T J, KADIR M F Z, et al. A conceptual review on polymer electrolytes and ion transport models. *Journal of Science: Advanced Materials and Devices*, 2018, **3:** 1–17.

[6] TAO C, GAO M, YIN B, et al. A promising TPU/PEO blend polymer electrolyte for all-solid-state lithium ion batteries. *Electrochimica Acta*, 2017, **257:** 31–39.

[7] JUNG H R, JU D H, LEE W J, et al. Electrospun hydrophilic fumed silica/polyacrylonitrile nanofiber-based composite electrolyte membranes. *Electrochimica Acta*, 2009, **54:** 3630–3637.

[8] KUPPU S V, JEYARAMAN A R, GURUVIAH P K, et al. Preparation and characterizations of PMMA-PVDF based polymer composite electrolyte materials for dye sensitized solar cell. *Current Applied Physics*, 2018, **18:** 619–625.

[9] ZHAI W, ZHU H, WANG L, et al. Study of PVDF-HFP/PMMA blended micro-porous gel polymer electrolyte incorporating ionic liquid [BMIM] BF_4 for lithium ion batteries. *Electrochimica Acta*, 2014, **133:** 623–630.

[10] VIGNAROOBAN K, DISSANAYAKE M A K L, ALBINSSON I, et al. Effect of TiO_2 nano-filler and EC plasticizer on electrical and thermal properties of poly(ethylene oxide) (PEO) based solid polymer electrolytes. *Solid State Ionics*, 2014, **266:** 25–28.

[11] VIJAYAKUMAR G, KARTHICK S N, SATHIYA PRIYA A R, et al. Effect of nanoscale CeO_2 on PVDF-HFP-based nanocomposite porous polymer electrolytes for Li-ion batteries. *Journal of Solid State Electrochemistry*, 2007, **12:** 1135–1141.

[12] CROCE F, SCROSATI B, MARIOTTO G. Electrochemical and spectroscopic study of the transport properties of composite polymer electrolytes. *Chem. Mater.*, 1992, **4:** 1134–1136.

[13] YAO P, ZHU B, ZHAI H, et al. PVDF/palygorskite nanowire composite electrolyte for 4 V rechargeable lithium batteries with high energy density. *Nano Letters*, 2018, **18:** 6113–6120.

[14] AHMAD S, AHMAD S, AGNIHOTRY S A. Nanocomposite electrolytes with fumed silica in poly(methyl methacrylate): thermal, rheological and conductivity studies. *Journal of Power Sources*, 2005, **140:** 151–156.

[15] JITJAICHAM M, KUSUKTHAM B. Spinning of poly(ethylene terephthalate) fiber composites incorporated with fumed silica. *Silicon*, 2017, **10:** 575–583.

[16] WANG J, KHOO E, LEE PS, et al. Synthesis, assembly, and electrochromic properties of uniform crystalline WO_3 nanorods. *J. Phys. Chem. C*, 2008, **112:** 14306–14312.

[17] ZHAO Q, FANG Y, QIAO K, et al. Printing of WO_3/ITO nanocomposite electrochromic smart windows. *Solar Energy Materials and Solar Cells*, 2019, **194:** 95–102.

[18] EL-FATTAH M A, El SAEED A. M, et al. Chemical interaction of different sized fumed silica with epoxy *via* ultrasonication for improved coating. *Progress in Organic Coatings*, 2019, **129:** 1–9.

[19] PUGUAN J M C, CHUNG W J, KIM H, et al. Ion-conductive and transparent PVDF-HFP/silane-functionalized ZrO_2 nanocomposite electrolyte for electrochromic applications. *Electrochimica Acta*, 2016, **196:** 236–244.

[20] SAIKIA D, WU C G, FANG J, et al. Organic-inorganic hybrid polymer electrolytes based on polyether diamine, alkoxysilane, and trichlorotriazine: synthesis, characterization, and electrochemical applications. *Journal of Power Sources*, 2014, **269(10):** 651–660.

[21] TANG Q, LI H, YUE Y, et al. 1-Ethyl-3-methylimidazolium tetrafluoroborate-doped high ionic conductivity gel electrolytes with reduced anodic reaction potentials for electrochromic devices. *Materials & Design*, 2017, **118:** 279–285.

[22] LEONES R, SABADINI R C, SENTANIN F C, et al. Polymer electrolytes for electrochromic devices through solvent casting and Sol-Gel routes. *Solar Energy Materials & Solar Cells*, 2017, **169:** 98–106.

[23] ZHANG F, DONG G, LIU J, et al. Polyvinyl butyral-based gel polymer electrolyte films for solid-state laminated electrochromic devices. *Ionics*, 2017, **23:** 1879–1888.

[24] RAGHAVAN S R, RILEY M W, FEDKIW P S, et al. Composite polymer electrolytes based on poly(ethylene glycol) and hydrophobic fumed silica: dynamic rheology and microstructure. *Chemistry of Materials*, 1998, **10(1):** 244–251.

[25] ŠURCA VUK A, JOVANOVSKI V, POLLET-VILLARD A, et al. Imidazolium-based ionic liquid derivatives for application in electrochromic devices. *Solar Energy Materials and Solar Cells*, 2008, **92 (2):** 126–135.

[26] BAE J, KIM H, MOON H C, et al. Low-voltage, simple WO_3-based electrochromic devices by directly incorporating an anodic species into the electrolyte. *Journal of Materials Chemistry C*, 2016, **46(4):** 10887–10892.

[27] CUI J, ZHOU Z, JIA M, et al. Solid polymer electrolytes with flexible framework of SiO_2 nanofibers for highly safe solid lithium batteries. *Polymers*, 2020, **12:** 1324.

基于高电导率的疏水气相 SiO$_2$ 复合凝胶电解质的
高性能电致变色器件

赵 起 [1]，乔 科 [1]，姚勇吉 [1]，陈 长 [1]，陈东初 [2]，高彦峰 [1]

(1. 上海大学 材料科学与工程学院, 上海 200444；2. 佛山大学 材料科学与能源工程学院, 佛山 528000)

摘　要：凝胶电解质具有化学稳定、难燃和易于封装等特点, 其低离子电导率(10^{-4}~10^{-5} S·cm^{-1})阻碍了电致变色器件(ECDs)凝胶电解质的进一步发展。本研究制备了一种高电导率的疏水 SiO$_2$/PMMA/PC/LiClO$_4$ 凝胶聚合物电解质(H-SiO$_2$ GPEs), 并用电化学阻抗谱(EIS)、循环伏安法(CV)和计时电流法(CA)分析了 ECDs 的电化学行为。实验结果表明, 仅引入 0.5wt%的疏水性气相 SiO$_2$, 即可使 H-SiO$_2$ GPEs 的离子电导率达到 5.14 mS·cm^{-1}(25 ℃时)。离子电导率的增加归因于 SiO$_2$ 添加物和有机电解质之间良好的相容性和疏水–疏水吸引力促进了高氯酸锂的离解。同时, 不同气相二氧化硅含量的 GPEs 的粘度与剪切速率的关系表现出剪切稀化行为, 这表明研究体系形成了三维网状结构。该结构为离子提供了传输通道, 进而提高了基于 H-SiO$_2$ GPEs 电致变色器件的响应速度($t_{bleaching}$= 4 *vs* 8 s 和 $t_{coloring}$ = 14 *vs* 16 s)。同样, 通过探究添加疏水性气相 SiO$_2$ 对液态电解液的影响表明：复合疏水性气相 SiO$_2$ 使得 LiClO$_4$/PC 液态电解液的离子电导率由原来的 6.94 mS·cm^{-1} 增大到 7.58 mS·cm^{-1}。疏水性气相 SiO$_2$ 作为填料对电解质的离子电导率具有一定的积极作用, H-SiO$_2$ GPEs 的研究为解决 ECDs 高离子电导率和易泄漏之间的矛盾提供了新思路。

关　键　词：凝胶电解质；电致变色；疏水性；SiO$_2$

中图分类号: TQ174　　**文献标识码**: A

Supporting materials:

High-conductivity Hydrophobic Fumed-SiO$_2$ Composite Gel Electrolyte for High Performance Electrochromic Devices

ZHAO Qi[1], QIAO Ke[1], YAO Yongji[1], CHEN Zhang[1], CHEN Dongchu[2], GAO Yanfeng[1]

(1. School of Materials Science and Engineering, Shanghai University, Shanghai 200444, China; 2. School of Materials Science and Energy Engineering, Foshan University, Foshan 528000, China)
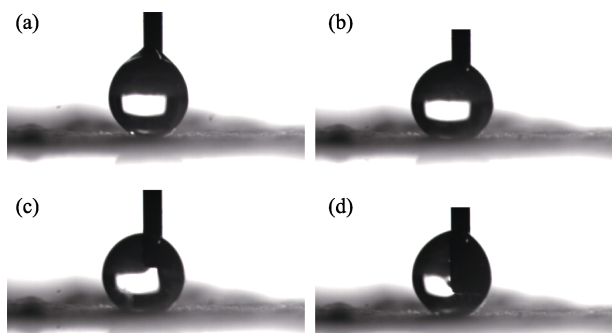
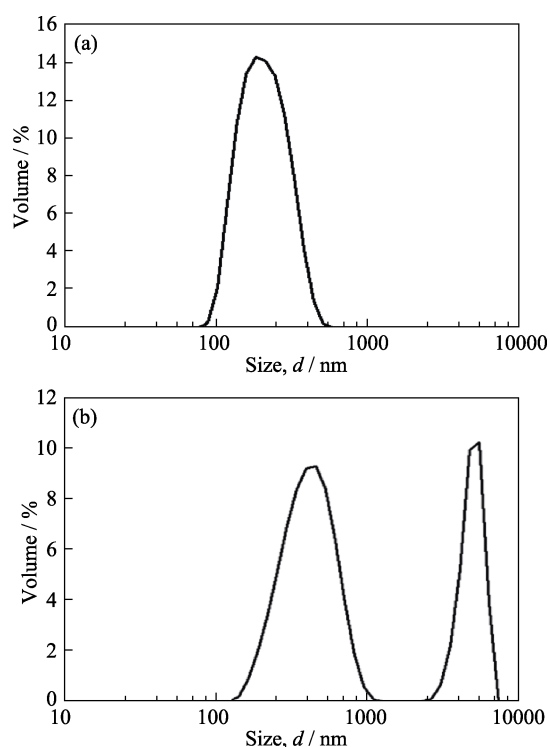Fig. S1　Static water contact angle (CA) of hydrophobic fumed SiO$_2$

Table S1　Ion conductivity of gel electrolytes from the literature

Electrolyte	Ionic conductivity/(mS·cm^{-1})
PMMA/LiClO$_4$/hydrophobic SiO$_2$ (This work)	5.14
PMMA/LiClO$_4$/hydrophilic SiO$_2$[1]	3.8
P(BMA-St)/hydrophilic SiO$_2$[2]	2.15
PEO/LiCF$_3$SO$_3$/TiO$_2$[3]	0.16
PVDF/LiClO$_4$/palygorskite[4]	0.12
PMMA/LiClO$_4$/[Emim]BF$_4$[5]	2.9
PVB/LiClO$_4$[6]	0.04
PVDF-HFP/LiCF$_3$SO$_3$/ZrO$_2$[7]	1.78
PAN/LiClO$_4$/Li$_{0.33}$La$_{0.557}$TiO$_3$[8]	0.0605

Fig. S2　Particle size of hydrophobic fumed silica (a) and hydrophilic fumed silica (b) in PC
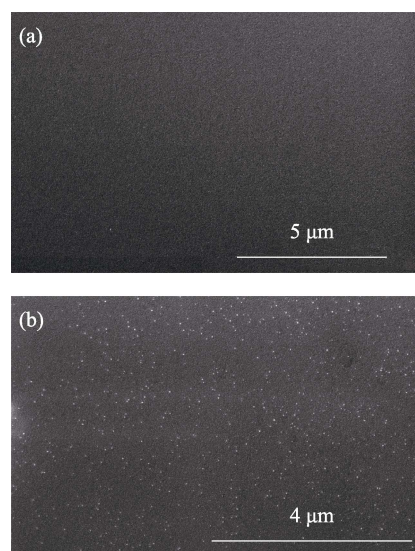

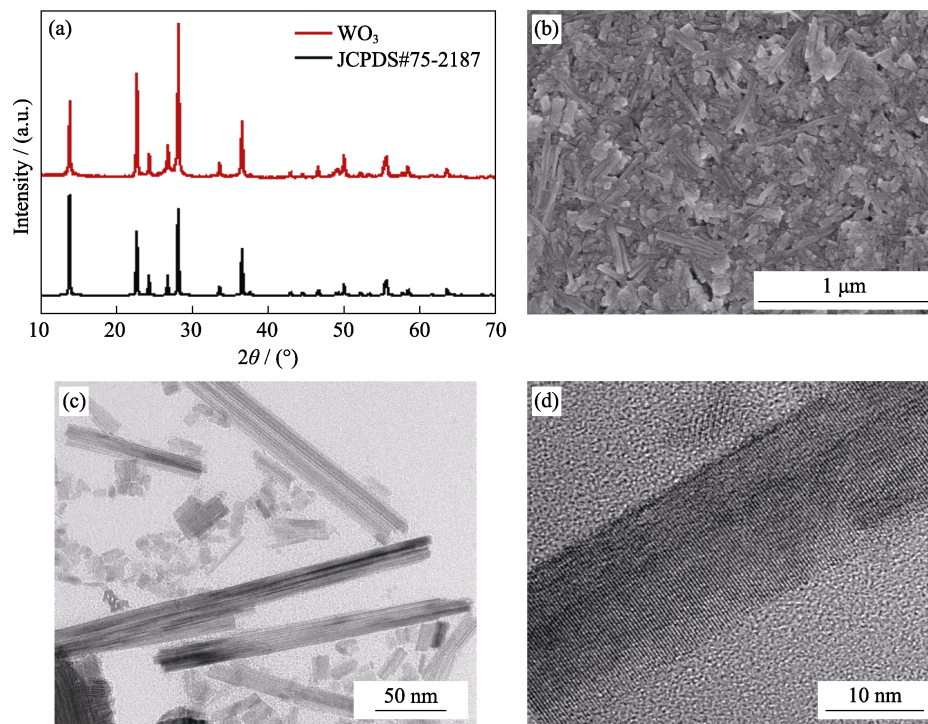Fig. S3　SEM images of pure GPEs (a) and 0.5wt% H-SiO$_2$ GPEs (b)

Fig. S4   XRD patterns of the as-prepared WO$_3$(a), SEM image of WO$_3$ films coated on ITO substrates(b), TEM images of WO$_3$ dispersion (c) and typical nanorod (d) with high magnification

References:

[1] AHMAD S, AHMAD S, AGNIHOTRY S A. Nanocomposite electrolytes with fumed silica in poly(methyl methacrylate): thermal, rheological and conductivity studies. *Journal of Power Sources*, 2005, **140:** 151–156.

[2] LIAO Y H, RAO M M, LI W S, *et al*. Fumed silica-doped poly(butyl methacrylate-styrene)-based gel polymer electrolyte for lithium ion battery. *Journal of Membrane Science*, 2010, **352:** 95–99.

[3] VIGNAROOBAN K, DISSANAYAKE M A K L, ALBINSSON I, *et al*. Effect of TiO$_2$ nano-filler and EC plasticizer on electrical and thermal properties of poly(ethylene oxide) (PEO) based solid polymer electrolytes. *Solid State Ionics*, 2014, **266:** 25–28.

[4] YAO P, ZHU B, ZHAI H, *et al*. PVDF/palygorskite nanowire composite electrolyte for 4 V rechargeable lithium batteries with high energy density. *Nano Letters*, 2018, **18:** 6113–6120.

[5] TANG Q, LI H, YUE Y, *et al*. 1-Ethyl-3-methylimidazolium tetrafluoroborate-doped high ionic conductivity gel electrolytes with reduced anodic reaction potentials for electrochromic devices. *Materials & Design*, 2017, **118:** 279–285.

[6] ZHANG F, DONG G, LIU J, *et al*. Polyvinyl butyral-based gel polymer electrolyte films for solid-state laminated electrochromic devices. *Ionics*, 2017, **23:** 1879–1888.

[7] PUGUAN J M C, CHINNAPPAN A, APPIAH-NTIAMOAH R, *et al*. Enhanced ionic conductivity and optical transmissivity of functionalized ZrO$_2$/PVdF-HFP hybrid electrolyte for energy efficient windows. *Solar Energy Materials and Solar Cells*, 2015, **137:** 265–273.

[8] LIU W, LEE S W, LIN D. Enhancing ionic conductivity in composite polymer electrolytes with well-aligned ceramic nanowires. *Nature Energy*, 2017, **2(5):** 17035.